Tellus (1999), 51A, 790–802
Printed in UK – all rights reserved

TELLUS
ISSN 0280–6495

Significant change of extratropical natural variability and potential predictability associated with the El Niño/Southern Oscillation

By WILBUR Y. CHEN* and HUUG M. VAN DEN DOOL, *Climate Prediction Center, NCEP/NWS/NOAA, 5200 Auth Road, Washington DC 20233, USA*

(Manuscript received 14 September 1998; in final form 1 March 1999)

ABSTRACT

Beyond the deterministic limit where the initial value sensitive predictability can hardly be found, the boundary condition dependent potential predictability is examined. The tropical anomalies of the opposite phases of El Niño/Southern Oscillation (ENSO) can significantly change the extratropical natural variability on a wide range of spatial and temporal scales. We address the impact on the low-frequency variability, such as the persistent blocking flows, and the high-frequency variability, represented primarily by the storm tracks. The NCEP/NCAR reanalyses are used for this investigation. Several diagnostics tools help to reveal the dynamical processes leading to the large change of the natural variability and the potential predictability in the extratropical latitudes between these two phases of the ENSO cycle. During El Niño winters, the principal storm tracks are steered more into the southern and Baja California region, by the much eastward extended subtropical jets. On the other hand, the storms are diverted more into the higher latitudes (Aleutians and Gulf of Alaska) during La Niña winters, when jetstreams are much weaker east of 160°W. Although being passively steered to widely different regions, the high-frequency transients do feed back actively to strengthen and maintain the subtropical jet across the central North Pacific and also act to slow down the equatorward flank of the jet. The feedback by the transients is stronger during the El Niño than the La Niña winters, helping in maintaining stronger signals from the tropics for the El Niño winters. There is also a large change of low-frequency variability: much larger magnitude of kinetic energy and height variance during La Niña than El Niño winters. The local barotropic energy diagnosis reveals that, on average, the low-frequency components extract more energy from time-mean flows during La Niña than El Niño winters, helping in explaining the presence of much larger low-frequency variability during the La Niña winters. With stronger ENSO signals and weaker natural variability during El Niño winters, the potential predictability in the north Pacific sector is significantly higher, on these two counts, than during the La Niña winters.

1. Introduction

The El Niño/Southern Oscillation (ENSO) phenomena (Rasmusson and Wallace, 1983) have attracted increasing attention. Its interannual variability influences many regions of the globe and is probably the most pronounced part of the climate variability. Our interest here is the ENSO related potential predictability for the extratropical atmosphere. We like to know whether there is a significant change in potential predictability from the warm to the cool phase of the ENSO cycle. In addition to ENSO signatures in the extratropical atmosphere, their magnitude and extent, we need to know whether there is a significant change in the amount of ENSO related

* Corresponding author.
e-mail: wchen@ncep.noaa.gov

noise or natural variability that accompanies the signals.

The natural variability in this article refers to fluctuations of various temporal and spatial scales while the atmosphere is subjected to a constant external forcing. For a perpetual general circulation model (GCM) experiment, the variability of all scales generated is easily understood to be natural variability, since the forcing is held constant. For the real atmosphere, however, not all variability is natural. In addition to repetitive annual cycle, the slowly varying anomalous external conditions inevitably generate additional variability. The total variability is therefore consisting of both externally forced and natural (Madden, 1976; Zwiers, 1987). Taking a seasonal mean of a meteorological variable for instance, its interannual variability consists of climate signal (externally forced) and climate noise. The latter always develop even when change of forcing is negligible (Lau, 1981). For high-frequency synoptic-scale transients, one can envision that the external forcings affect at least the location of their principal tracks. The external forcing can also affect the magnitude of natural variability of low-frequency fluctuations.

Isolating climate signal from noise in the real atmosphere is known to be formidable, if not impossible (Leith, 1973; Madden, 1976; Trenberth, 1985; Chervin, 1986). The emphasis of this article is not on a precise way to separate them. We attempt to understand a simpler situation. When the external condition changes from El Niño to La Niña type of forcing, we are asking whether there is a corresponding change in magnitude of natural variability? Since the variance of natural variations is closely related to the potential predictability (Madden, 1976; Chervin, 1986), our goal is to find out whether there is a substantial impact of tropical SST anomalies on the extratropical atmospheric natural variability and potential predictability.

The response of time-mean flow to external forcing has been well documented and qualitatively understood in various frameworks (Opsteegh and Van den Dool, 1980; Hoskins and Karoly, 1981; Horel and Wallace, 1981; Shukla, 1983; Blackmon et al., 1983; Cubasch, 1985; Miyakoda et al., 1986; Barnett, 1995; Kumar et al., 1996). However, to what extent a tropical forcing modifies the natural variability is less clear. If a large modification is evident, what then could be the dynamical processes that lead to the change? Because of the omnipresence of natural variability, the ENSO potential predictability will always have an upper limit. While climate signals contribute positively to the predictability, the presence of climate noise can only diminish it. We attempt to gain further understanding on the cause and nature of the extratropical atmospheric natural variability and potential predictability.

In this continuing effort, some preliminary results have been obtained using a limited set of operational analyses (Chen and Van den Dool, 1995 and 1997a) and a set of general circulation model experiments (Chen and Van den Dool, 1997b). Adopting a slightly different technique, Lin and Derome (1997) have also reported a modification of natural variability by the large-scale environments. Recently, the National Centers for Environmental Prediction (NCEP) and the National Center of Atmospheric Research (NCAR) have jointly accomplished an extremely valuable reanalysis (Kalnay et al., 1996). Exploiting these consistent and voluminous new data, especially the global coverage and full length of wind fields that were not available for our earlier attempts, we conduct a revisit of the above issue. The tropical and subtropical data available for this study contribute tremendously to the insights we have been attempting to gain.

2. Data and warm/cool ENSO seasons

The data used are the new NCEP/NCAR reanalyses (Kalnay et al., 1996). The wind and geopotential height fields at 200, 500, and 700 mb levels from 1961 to 1997 are investigated. For this study, we focus on the wintertime seasons. Data from 1 October to 30 April were extracted first and the 37-year climatology obtained and anomaly fields formed. Because of temporal filtering that will be described in more detail later, the final data sets used are shorter, from 1 December to 31 March, referred to hereafter as DJFM winter season.

The warm and cool phases of the ENSO cycles were sorted out from the sea surface temperature (SST) anomalies in the Niño 3.4 region (5S–5N and 120–170W). The NCEP's SST operational analysis and re-analysis for earlier periods (1950–92, Smith et al. 1996) were used for this purpose. Fig. 1 dis-

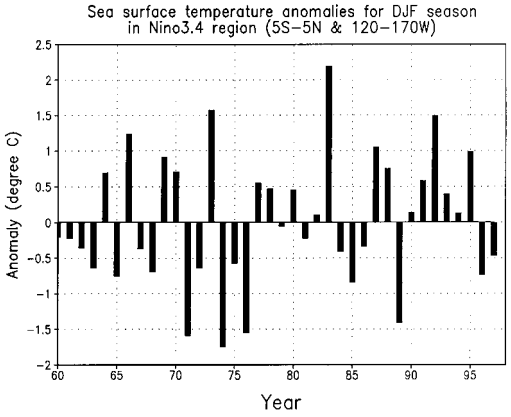

Fig. 1. Year-to-year variations of sea surface temperature anomaly in Niño 3.4 region. The DJF climatology is based on the period of 1950 to 1997.

plays the year-to-year variations of the DJF-mean Niño 3.4 SST anomalies. With a criterion of exceeding 0.75°C in SST anomaly, 7 warm El Niño seasons as well as 7 cool La Niña seasons were objectively identified. The warm cases are (using January for year identification): 1966, 1969, 1973, 1983, 1987, 1992, and 1995; and the cool seasons are: 1965, 1971, 1974, 1976, 1985, 1989, and 1996.

3. ENSO signals

Responding to tropical El Niño/La Niña anomalies, the Northern Hemispheric upper level jetstreams undergo large change, as shown in Fig. 2. The El Niño DJFM composites are shown in the left panels while the La Niña seasons in the right. The top panels compare the strength of the 200 mb zonal winds. We see a large difference in the eastern half of the North Pacific. For El Niño winters, the mean jet extends much farther eastward with speed greater than 30 m/s and merges with the branch over the United States. For La Niña winters, the mean jet is rather weak over the vast eastern North Pacific.

The composites of wind vector anomaly for El Niño and La Niña winters are contrasted in the middle panels. For El Niño winters, accompanying the jet's eastward extension, there is a large tropical easterly anomaly with magnitude exceeding 5 m/s. Therefore, an anticyclonic anomaly circulation over the subtropical ocean east of the date line is clearly seen. In fact, the well known Pacific North American (PNA) teleconnection pattern (Horel and Wallace, 1981; Wallace and Blackmon, 1983; Barnston and Livezey, 1987) is clearly observable: in addition to the subtropical anticyclonic center, there is a cyclonic anomaly center in the northeast Pacific, a strong anti-cyclonic anomaly circulation center over the central Canada, and a weak cyclonic center off shore from south Atlantic coast. For the La Niña winters, the composite (the middle right panel) reveals a near reversal of the above teleconnection pattern. However, the Canadian cyclonic circulation anomaly is much weaker than its counterpart of the El Niño composite.

The Z500 anomaly composites are contrasted in the bottom panels. In simple contours they depict essentially the same circulation anomalies of the middle panels. Since the composites were averaged from 7 El Niño/La Niña events, eliminating most of the natural variability, we loosely treat these means as the ENSO signatures. Based on this treatment, we see that the tropical El Niño anomalies imprint a stronger signature on the Pacific North American (PNA) sector during El Niño winters than the La Niña winters. The El Niño signal over Eastern Canada is notably much stronger. The La Niña signal in the north Pacific is seen to be weaker and elongated northwestwards to Kamchatka.

4. Subseasonal natural variability

Embedded in the ENSO signal is natural variability on a wide range of spacial and temporal scales. Daily synoptic disturbances and persistent blocking flows are familiar examples. In the following, we present: (a) high-frequency variability (HFV) with time-scales less than 7 days, representing the main storm tracks; (b) low-frequency variability (LFV) with time-scales between 11 and 61 days, consisting of persistent blocking highs and large-scale deep trough flows.

4.1. Modification of HFV

In general, the principal storm tracks are located on the northern flank of the jetstreams and assume an elongated distribution across the North Pacific (Blackmon et al., 1977). Although the storm tracks are not directly forced by the tropical anomalies,

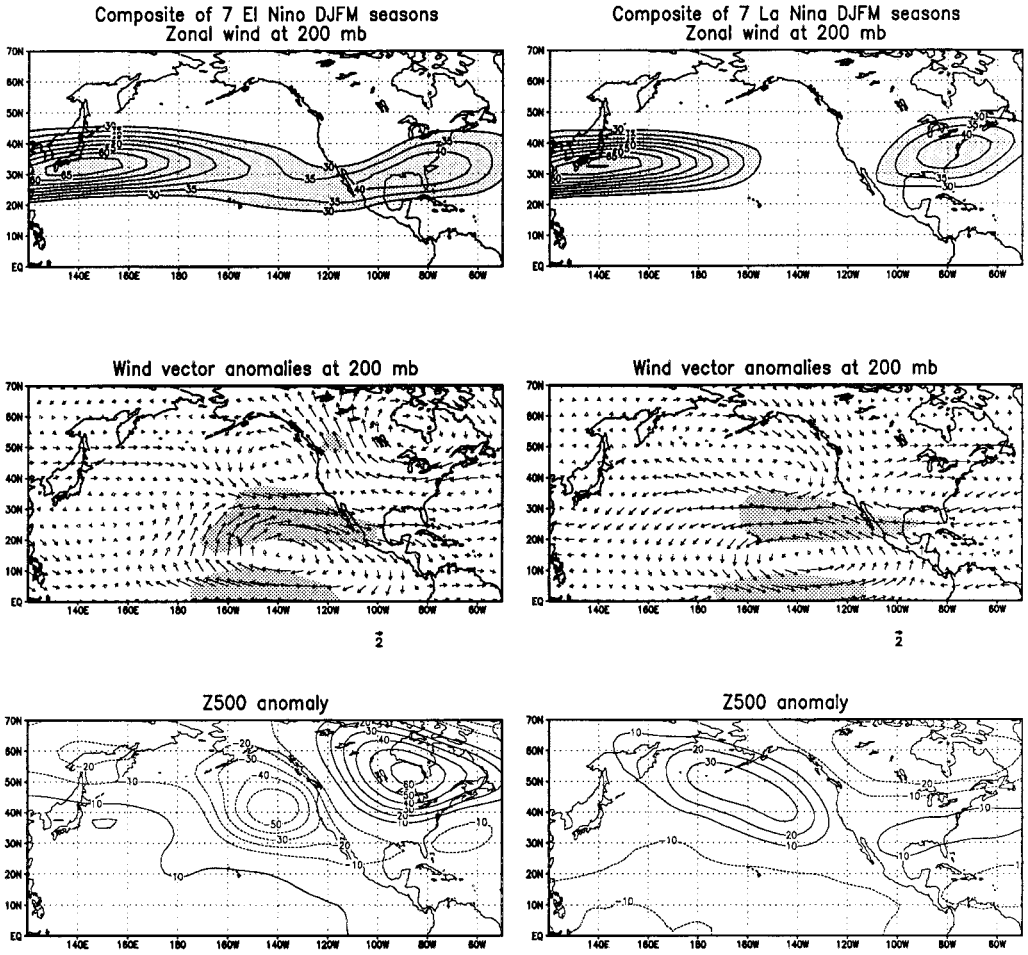

Fig. 2. Composites of DJFM wind (m/s) and height (m) fields. El Niño years are: 1966, 69, 73, 83, 87, 92, and 95. La Niña years are: 1965, 71, 74, 76, 85, 89, and 96. Wind vector anomalies greater than 5 m/s are shaded. Bottom panels, solid (dashed) contours are for positive (negative) Z500 anomalies.

they are steered by the time-mean flows (Lau, 1988). With so much difference in the strength of the zonal mean flows between El Niño and La Niña winters as seen in Fig. 2, we expect a large difference in the geographical distribution of the principal storm tracks.

Following the method of describing the principal storm tracks by Nakamura and Wallace (1990), we isolate first the high-frequency fluctuations of the 700 mb meridional wind by applying a 7-day running mean high-pass filter over the DJFM time series. In order to avoid being contaminated by the end-effect of the filtering, 3 more data points at both ends have been added before filtering. After squaring the high-pass filtered fluctuations and raising the values by a factor of 2 and finally low-pass filtering by a 7-day running mean, we obtain the envelop of the storm tracks, in the same manner as used by Nakamura and Wallace (1990). The top panel of Fig. 3 presents the climatological (1961–97) distribution of the storm tracks for the DJFM seasons. The tracks are zonally elongated across the ocean and located mainly on the northern flank of the mean jet, agreeing well with previous results (Blackmon et al., 1977).

The lower two panels reveal the departures from

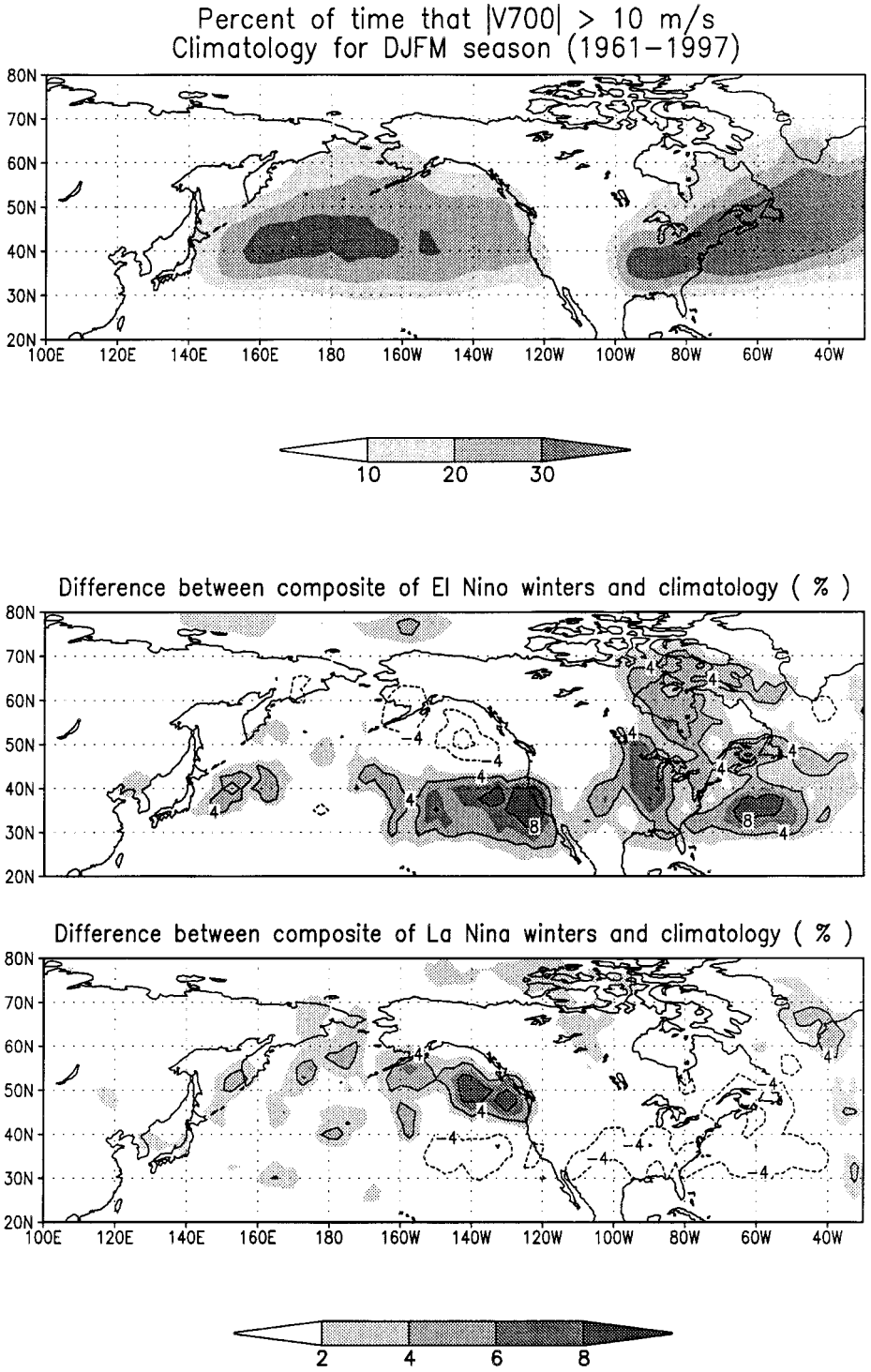

Fig. 3. Principal storm tracks represented by 7-day high-pass filtered and large meridional winds at 700 mb. See text for detail procedures to obtain them. Top panel is the 37-year climatology (1961–97) of the % of time that a filtered |V700| is greater than 10 m/s. Other two panels show the difference of % between the El Niño/La Niña composite and the climatology. Contour interval is 4%. Solid (dashed) curves for increase (decrease) in %.

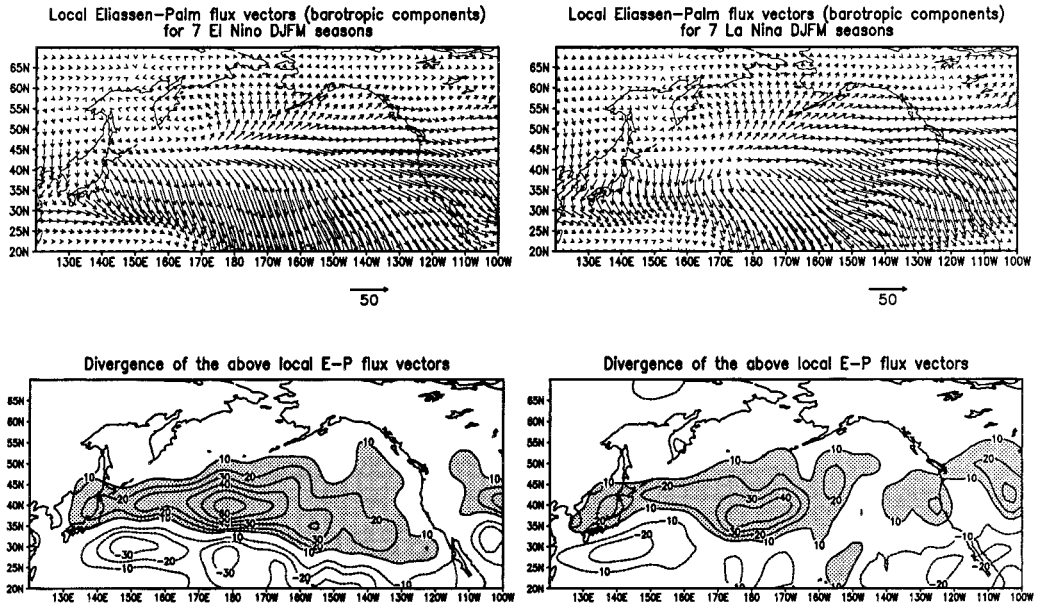

Fig. 4. Composites of the barotropic components of the local Eliassen–Palm flux vectors ($m^2\ s^{-2}$) at 200 mb (top panels) and their divergence ($m\ s^{-1}$/day) (bottom panels). Solid (dashed) contours for divergence (convergence).

the climatological storm tracks for, separately, the El Niño and La Niña winters. For the former (the middle panel), the storms are steered by the eastward extended jet to reach the southern/Baja California region, bringing heavy precipitation into this climatologically semi-arid area. On the other hand, we see a deficit in storm activity over the vast region of northeastern Pacific. In sharp contrast, the La Niña anomalies (the bottom panel) show more storms being diverted northeastward to the northern edge of the North Pacific. Due to the retracted jetstream, the storm activity is much below normal across the central North Pacific between 30°N and 40°N, which is a large difference from the El Niño winters. Over the eastern half of the US, we see a sharp difference, with enhanced (decreased) storminess in El Niño (La Niña) winters.

It is apparent that the ENSO's warm/cool anomalies modify drastically the HFV of the extratropical atmosphere.

4.2. *High-frequency transient forcing of the time-mean flows*

Although the storm tracks are steered by the time-mean flows, they are not entirely a passive variable. They in fact positively feed back to maintain the time-mean flow (Holopainen et al., 1982; Hoskins et al., 1983; Shutts, 1983; Trenberth, 1986), even when the time-mean differs from climatology (Lau, 1988; Cai and Van den Dool, 1992). Following the diagnostics of the local Eliassen–Palm (EP) flux vector, modified by Trenberth (1986), we calculate the flux vectors and their divergence to get a feel of the interactions between the transients and the time-mean flows during different phases of the ENSO cycle. When the localized EP flux vectors are divergent, the effect of the transients is to force and maintain the time-mean flow (Trenberth, 1986).

The 7-day high-pass filtered wind components are used to construct the barotropic part of the EP flux vector, which is

$$E_u = [\tfrac{1}{2}(\langle v'^2\rangle - \langle u'^2\rangle);\ -\langle u'v'\rangle]$$

(Trenberth, 1986). The composites of E_u vectors and their divergence are shown in the left-hand panels of Fig. 4 for the 7 El Niño seasons, and the right-hand panels the 7 La Niña winters. The divergence in the lower panels reveal that the HVFs act to strengthen and maintain the subtropical jet across the central North Pacific, but, act to slow down the equatorward flank of the jet.

The forcing of the transients during El Niño winters is seen much stronger, both across the central North Pacific and in the deep tropics. The feedback of the transients help in maintaining stronger presence of El Niño signal than La Niña signal from the tropics.

4.3. *Modification of subseasonal low-frequency variability*

The low-frequency variability (LFV) with time-scales between 11 and 61 days are next investigated to see how they are modified by the ENSO tropical anomalies. The new reanalyses make investigations on variables other than Z500 (Chen and Van den Dool, 1997a) possible. We emphasize that the LFV considered here are those embedded in the ENSO signal, not the subseasonal anomalies from the climatological mean, which is substantially contaminated by the ENSO signal. Fig. 5 illustrates the embedding of the LFVs. The 11-day low-pass filtered Z500 anomalies are shown by the closed circles, for a La Niña (upper panel) and an El Niño DJFM season (lower panel), at grid point 45°N and 160°W, representing the general situation in the North Pacific. These low-pass filtered time series are consisting of ENSO signals as well as subseasonal natural variability. Because there is no clear spectral gap, it is impossible to separate the two with certainty. Our approach is to break the total variance into two groups in a poor man's fashion by applying a 61-day filter. Those with time-scales greater than 61 days are more likely to be the ENSO signals (the dashed curves in Fig. 5), while those less than 61 days the natural variability. There is no solid reason for

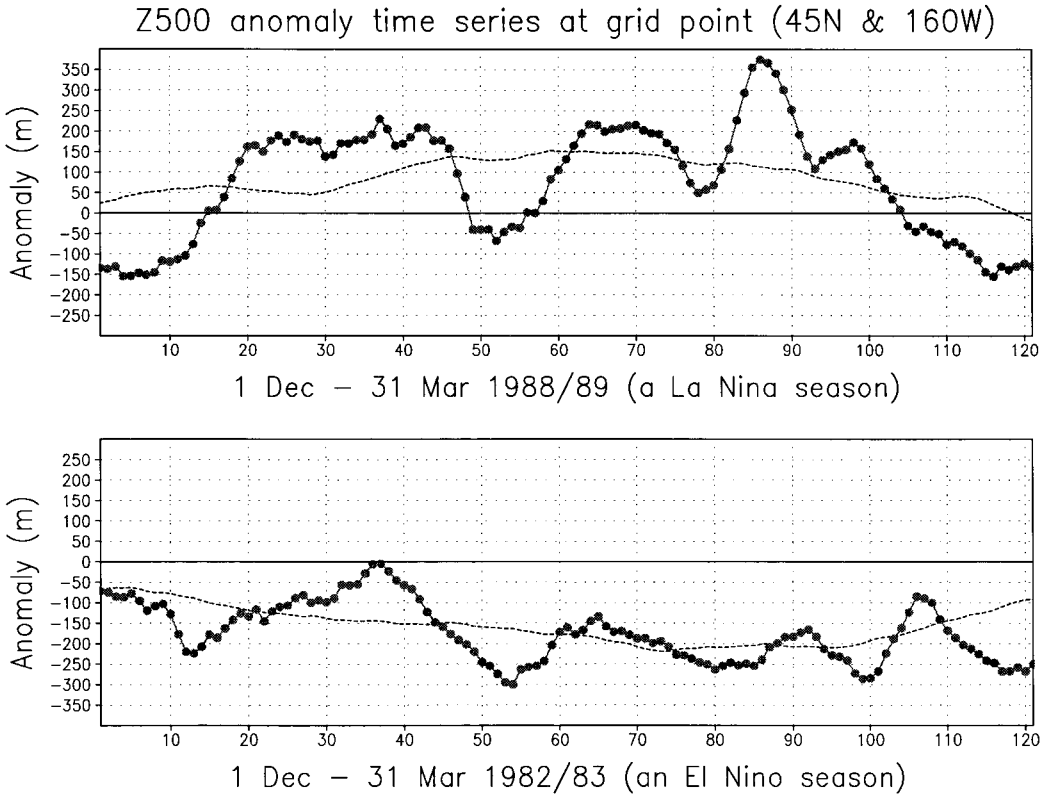

Fig. 5. Illustration of Z500 anomaly time series at grid point (45°N and 160°W), showing time-mean flow (dashed curve) and the embedded low-frequency disturbances (departures of closed circles from dashed curve), separately for a cool (1988/89) and a warm (1982/83) DJFM season. A 61-day (11-day) low-pass filter was applied to obtain the dashed (close-circled) curves.

using a 61-day filter except for the considerations of: (a) the persistent blocking and deep trough flows are most likely to develop in the range of 11–61 days, and 61-day is close to a seasonal time scale; (b) it is short enough to let the signals stand out more to reveal their intraseasonal evolution. The ENSO signal extracted in this fashion overestimates its magnitude, because there is natural variability with time scales longer than 61 days. By averaging over more and more cases one can eliminate some uncertainty and gradually improve the estimate of ENSO signal.

The LFVs considered here are then those departures from the dashed curves, not the anomalies from the climatology, as used in some of the studies on persistent anomalies (Dole, 1986). The LFVs considered here better represent natural variability while the low-frequency departures from climatology contain both interannual signals and natural variability. From the illustrations of Fig. 5, we can visualize that the LFVs considered here are indeed those embedded in the loosely defined ENSO signal.

Fig. 6 contrasts the kinetic energy of the LFVs at 200 mb for the El Niño winters (left panel) and the La Niña winters (right panel). A comparison for Z500 variance is shown in the lower panels. It is apparent from the figure that there is a large difference in LFVs: much larger magnitude of kinetic energy and height variance for the La Niña winters than the El Niño winters. If one had used the conventional climatological anomalies to obtain the above quantities, there would have been little difference between them. The immediate question is why there is so much difference in LFV kinetic energy and height variance between the warm and cool phase of the ENSO cycles. What is the dynamical process leading to this large change?

4.4. *Interaction between LFV and ENSO signal*

One plausible mechanism is explored here. We focus on the interactions between ENSO signals and the embedded LFV components. Simmons et al. (1983) and Palmer (1988) suggest that much of the low-frequency variability of the Northern Hemisphere wintertime general circulation is associated with disturbances which derive their energy from the zonally varying basic state through barotropic instability. It is then plausible that the local barotropic energy conversion between the zonally

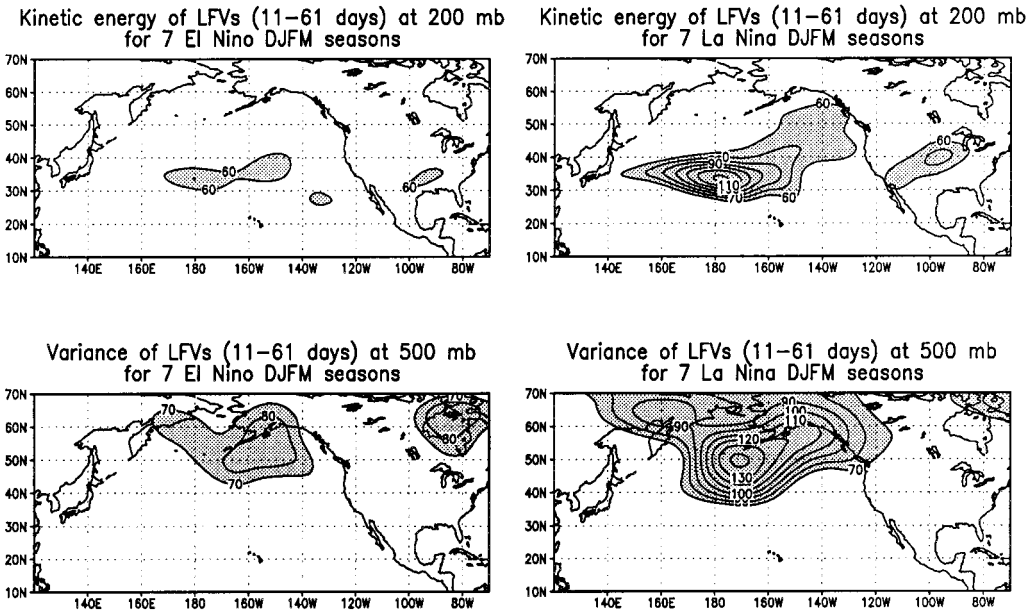

Fig. 6. Contrast of kinetic energy and Z500 variance of low-frequency components between El Niño and La Niña composites. Kinetic energy in $m^2\,s^{-2}$ and height variance in $(dm)^2$.

varying time-mean flows and the low-frequency components may account for the large difference shown in Fig. 6.

Using the notations and definitions of Mak and Cai (1989), the growth rate of the local perturbation energy is governed in large part by the scalar product, $\boldsymbol{E}\cdot\boldsymbol{D}$, in the following equation:

$$\varepsilon_t = -\boldsymbol{V}\cdot\nabla\varepsilon + \boldsymbol{E}\cdot\boldsymbol{D} - 2r\varepsilon - v\cdot\nabla p, \tag{1}$$

where

$$\varepsilon = \tfrac{1}{2}(u^2+v^2), \qquad \boldsymbol{v} = (u, v), \qquad \boldsymbol{V} = (U, V),$$

and

$$\boldsymbol{E} = (\tfrac{1}{2}(v^2-u^2), -uv), \tag{2}$$

$$\boldsymbol{D} = (U_x - V_y, V_x + U_y). \tag{3}$$

As discussed by Mak and Cai (1989), the mean-flow advection of the perturbation energy and the ageostrophic pressure work do not contribute to the change of the global energetics, but redistribute the perturbation energy and determine the location and localization of the disturbances. The $\boldsymbol{E}$-vector quantifies the local structure and the strength of the LFVs, while the $\boldsymbol{D}$-vector defines the deformation field of the ENSO signals in which the LFVs are embedded.

To evaluate the barotropic energy conversion between the ENSO signals and the LFVs, we treat the slowly evolving time-mean flows (TMFs), as illustrated in Fig. 5, as the ENSO signals and the embedded disturbances of time scales between 11 and 61 days as the LFV components (Chen and Van den Dool, 1995 and 1997a). The $\boldsymbol{E}$-vector was calculated through (2) and the $\boldsymbol{D}$-vector through (3) by using finite difference. The average inner product, $\boldsymbol{E}\cdot\boldsymbol{D}$, is shown in Fig. 7. The top panel displays the average of all 37 years considered, with positive (negative) contours indicating gaining (losing) of LFV kinetic energy from ENSO signals (the TMFs). A maximum energy conversion from signals to LFVs takes place in central north Pacific, near the exit region of the jetstream and extending eastward with weaker conversion through southern California into central United States. The difference in $\boldsymbol{E}\cdot\boldsymbol{D}$ between El Niño/La Niña winters and the climatological mean is shown in the lower two panels. The major features are: (a) during La Niña winters, there is much more TMF to LFV conversion along jetstreams except the central eastern North Pacific, where jetstreams extend into southern and Baja California during El Niño winters; (b) the positive conversion over western Canada is also larger for the La Niña winters. The above results are remarkably in sync with the large difference in LFV kinetic energy shown in Fig 6. What we see from these results is: during La Niña winters, there is much more LFV kinetic energy in central and northeastern Pacific, plausibly due to much more ENSO signal to LFV energy conversion.

5. Extratropical potential predictability

The above results indicate that much larger low-frequency natural variability is observed for the La Niña than the El Niño winters in the central and northeastern Pacific. Similar behavior is expected of the natural variability on seasonal time scales, because the energy spectral shape cannot change much from low-frequency to seasonal time scale. The reason we address the 11–61 days time scales is due to the consideration that the persistent blocking and deep trough flows (Chen and Van den Dool, 1997a) are mostly within this range.

From Fig. 2 we recall that ENSO signals are stronger for El Niño than La Niña winters. The potential predictability for the North Pacific atmosphere, on *seasonal time scales*, should then be higher for the El Niño winters than the La Niña winters. The potential predictability in terms of Z500 variability, i.e.,

$$\text{potential predictability} = \frac{\text{square of signal}}{\text{square of signal} + \text{variance of LFV}}$$

is obtained and shown in Fig. 8. We see, indeed, much higher potential predictability for the El Niño winters in the northeastern Pacific. The northeastern North America and the western subtropical Pacific also have much higher potential predictability for the El Niño winters. This result agrees fairly well with those of the general circulation model study of Chen and Van den Dool (1997b).

6. Conclusions

The new NCEP/NCAR reanalyses are investigated for the ENSO signal and its embedded

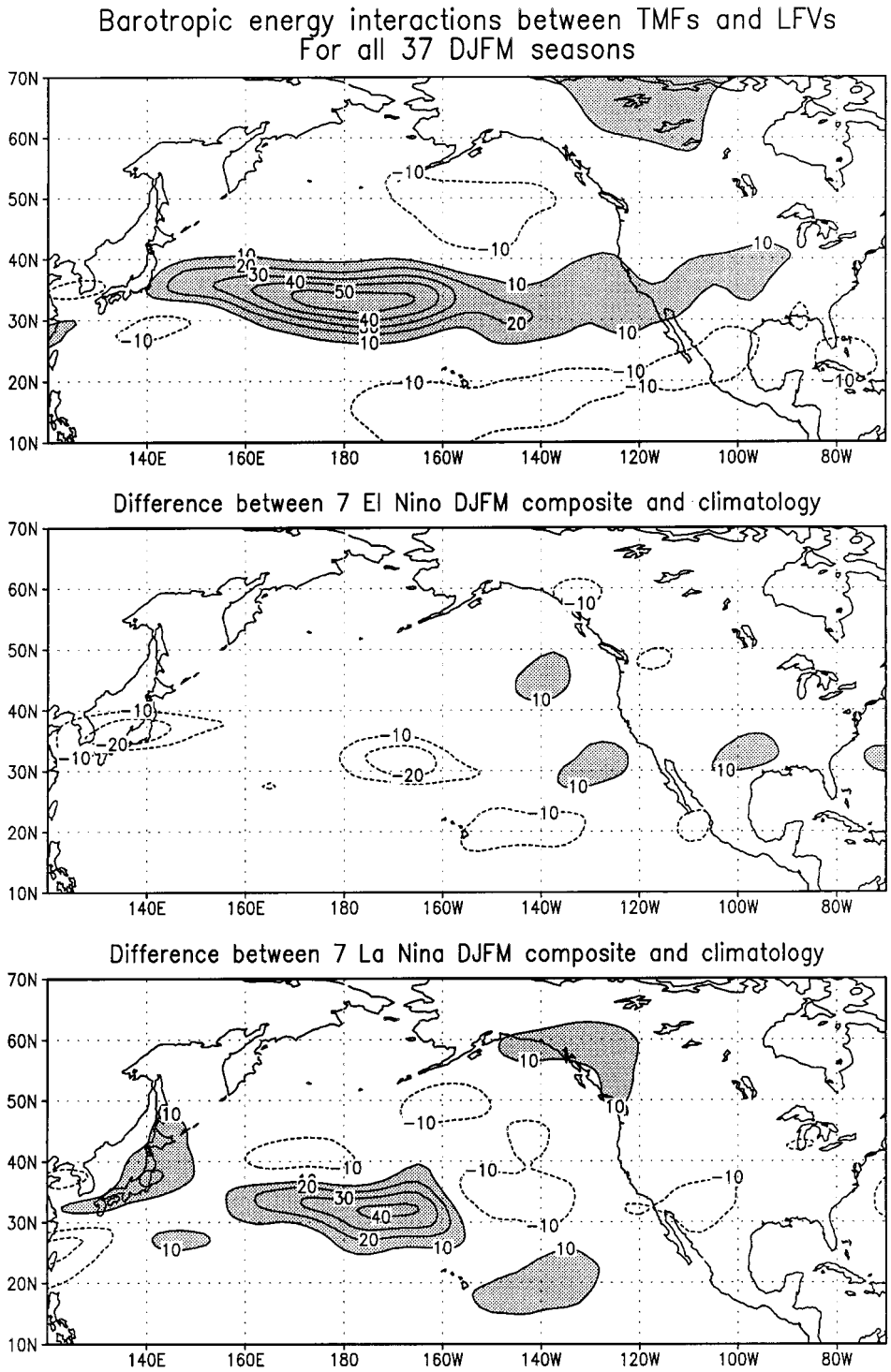

Fig. 7. Comparisons of barotropic energy conversions between ENSO signals and the embedded low-frequency perturbations. The unit of the scalar product, $\boldsymbol{E} \cdot \boldsymbol{D}$, is in $m^2\,s^{-2}$/day. Positive contours indicate conversion from time-mean flow to low-frequency disturbances.

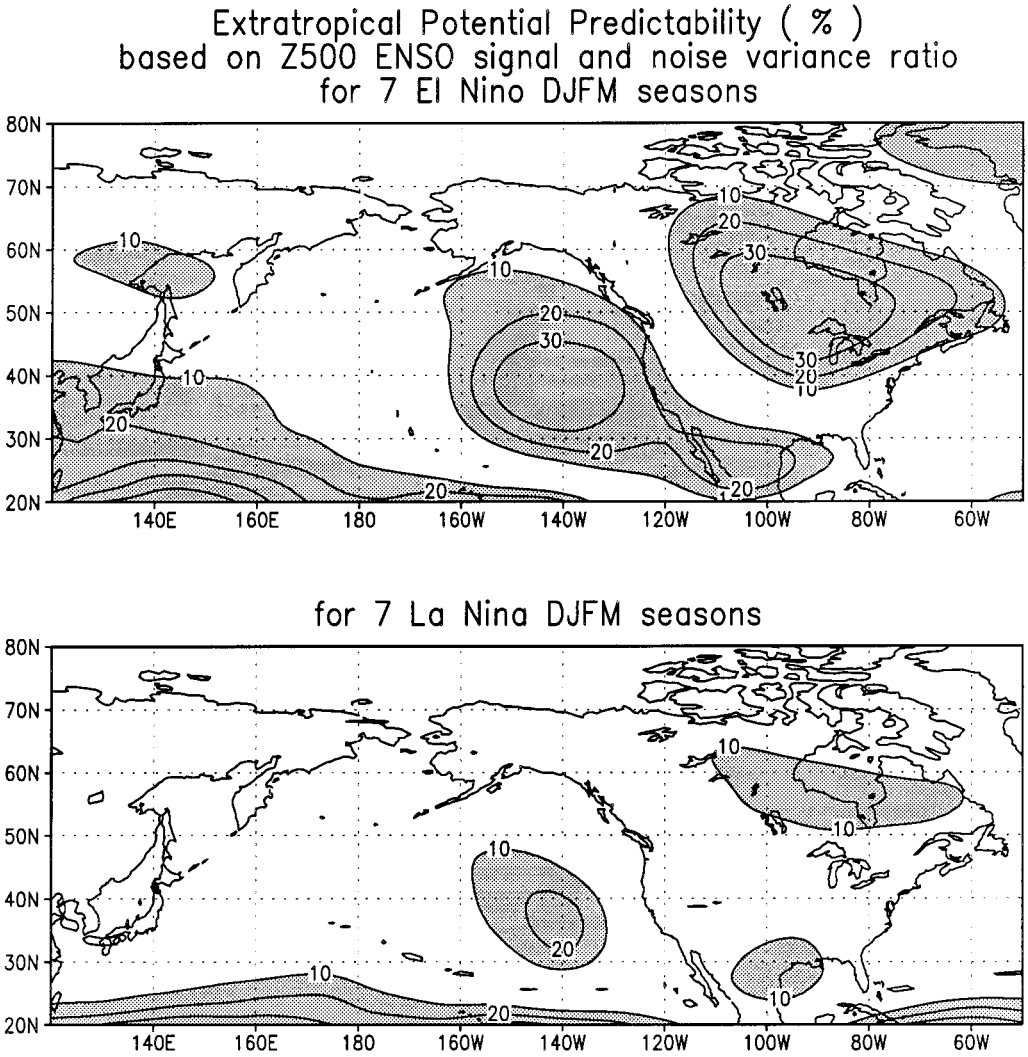

Fig. 8. Contrast of Z500 potential predictability (PP) between El Niño and La Niña DJFM.

natural variability in order to gain further understanding on extratropical potential predictability. Based on the climatology of period from 1961 to 1997, we find stronger ENSO signals for the El Niño than the La Niña type of external forcing. The 7-winter composites exhibit stronger ENSO signatures for the El Niño winters in both the northeastern Pacific and the northeastern North America (Fig. 2).

By excluding most of the ENSO signals from the total low-frequency variability, the climate noise is contrasted for the warm and the cool phases of the ENSO cycle. Much larger magnitude of low-frequency natural variability is found for the La Niña winters. A plausible dynamical explanation is explored. Because of large difference in time-mean deformation fields between warm and cool phase of the ENSO cycle, the extent of interactions between time mean flows and low-frequency components exhibits a large difference: much larger low-frequency variability for the La Niña than the El Niño extratropical atmosphere (Fig. 7).

On these two counts — stronger signals and

weaker low-frequency natural variability — significantly higher potential predictability in North Pacific sector follows as a consequence for the El Niño winters. The results presented here clearly indicate that the tropical ENSO anomalies do significantly change the characteristics of the natural variability as well as the ENSO potential predictability in the northern extratropical latitudes from one phase of the ENSO cycle to the other phase of the cycle.

7. Acknowledgments

The authors would like to acknowledge the tremendous contribution of the NCEP/NCAR reanalysis team headed by Drs. Eugenia Kalnay and Masao Kanamitsu. Without the reanalysis data, this study would not have been possible. They are also grateful to Dr. Vernon Kousky and two anonymous reviewers for their insightful comments that improve the quality of this paper.

REFERENCES

Barnett, T. P. 1995. Monte Carlo climate forecasting. *J. Climate* **8**, 1005–1022.

Barnston, A. G. and Livezey, R. E. 1987. Classification, seasonality and persistence of low-frequency atmospheric circulation patterns. *Mon. Wea. Rev.* **115**, 1083–1126.

Blackmon, M. L., Wallace, J. M., Lau, N.-C. and Mullen, S. L. 1977. An observational study of the Northern Hemisphere wintertime circulation. *J. Atmos. Sci.* **34**, 1040–1053.

Blackmon, M. L., Geisler, J. E. and Pitcher, E. J. 1983. A general circulation model study of January climate anomaly patterns associated with interannual variation of equatorial Pacific sea surface temperatures. *J. Atmos. Sci.* **40**, 1410–1425.

Cai, Ming and Huug van den Dool. 1992. Low-frequency waves and traveling storm tracks. Part II: Baroclinic component. *J. Atmos. Sci.* **49**, 2506–2524.

Chen, Wilbur Y. and Huug van den Dool. 1995. Low frequency variabilities for widely different basic flows. *Tellus* **47A**, 526–540.

Chen, Wilbur Y. and Huug van den Dool. 1997a. Asymmetric impact of tropical SST anomalies on atmospheric internal variability over the north Pacific. *J. Atmos. Sci.* **54**, 725–740.

Chen, Wilbur Y. and Huug van den Dool. 1997b. Atmospheric predictability of seasonal, annual, and decadal climate means and the role of the ENSO cycle: a model study. *J. Climate* **10**, 1236–1254.

Chervin, R. M. 1986. Interannual variability and seasonal climate predictability. *J. Atmos. Sci.* **43**, 233–251.

Cubash, U. 1985. The mean response of the ECMWF global model to the composite El Niño anomaly in the extended range prediction experiments. *Coupled ocean–atmosphere models* (ed. Nihoul, J.). Elsevier Science, pp. 329–344.

Dole, R. M. 1986. Persistent anomalies of the extratropical Northern Hemisphere wintertime circulation: Structure. *Mon. Wea. Rev.* **114**, 178–207.

Holopainen, E. O., Rontu, L. and Lau, N.-C. 1982. The effect of large-scale transient eddies on the time mean flow in the atmosphere. *J. Atmos. Sci.* **39**, 1972–1984.

Horel, J. D. and Wallace, J. M. 1981. Planetary scale atmospheric phenomena associated with the Southern Oscillation. *Mon. Wea. Rev.* **109**, 813–829.

Hoskins, B. J. and Karoly, D. J. 1981. The steady linear response of a spherical atmosphere to thermal and orographic forcing. *J. Atmos. Sci.* **38**, 1179–1196.

Hoskins, B. J., James, I. and White, G. H. 1983. The shape, propagation, and mean flow interaction of large-scale weather systems. *J. Atmos. Sci.* **40**, 1595–1612.

Kalnay, E., Kanamitsu, M. et al. 1995. The NCEP/NCAR 40-year reanalysis project. *Bull. Amer. Meteo. Soc.* **77**, 437–471.

Kumar, A., Hoerling, M., Ji, M., Leetmaa, A. and Sardeshmukh, P. 1996. Assessing a GCM's suitability for making seasonal predictions. *J. Clim.* **9**, 115–129.

Lau, N. C. 1981. A diagnostics study of recurrent meteorological anomalies appearing in a 15-year simulation with a GFDL general circulation model. *Mon. Wea. Rev.* **109**, 2287–2311.

Lau, N. C. 1988. Variability of the observed midlatitude storm tracks in relation to low-frequency changes in the circulation patterns. *J. Atmos. Sci.* **45**, 2718–2743.

Leith, C. E. 1973. The standard error of time-average estimates of climatic means. *J. Appl. Meteorol.* **12**, 1066–1069

Lin, H. and Derome, J. 1997. On the modification of the high- and low-frequency eddies associated with the PNA anomaly: an observational study. *Tellus* **49A**, 87–99.

Madden, R. A. 1976. Estimates of the natural variability of time-averaged sea-level pressure. *Mon. Wea. Rev.* **104**, 942–952.

Mak, M. and Cai, M. 1989. Local barotropic instability. *J. Atmos. Sci.* **46**, 3289–3311.

Miyakoda, K., Sirutis, J. and Ploshay, J. 1986. One-month forecast experiments — without anomaly boundary forcings. *Mon. Wea. Rev.* **114**, 2363–2401.

Nakamura, H. and Wallace, J. M. 1990. Observed changes in the baroclinic wave activity during the life cycles of low-frequency circulation anomalies. *J. Atmos. Sci.* **47**, 1100–1117.

Opsteegh, J. D. and van den Dool, H. M. 1980. Seasonal differences in the stationary response of a linearized

primitive equation model: Prospects for long-range weather forecasting? *J. Atmos. Sci.* **37**, 2169–2185.

Palmer, T. N. 1988. Medium and extended range predictability and stability of the Pacific/North American mode. *Quart. J. Roy. Met. Soc.* **114**, 691–713.

Rasmusson, E. M. and Wallace, J. M. 1983. Meteorological aspects of the El Niño/Southern Oscillation. *Science* **222**, 1195–1202.

Shukla, J. 1983. *On physical basis and feasibility of monthly and seasonal prediction with a large GCM*. Long-range forecasting research publications series, no. 11. WMO, 142–153.

Shutts, G. J. 1983. The propagation of eddies in diffluent jet streams: Eddy vorticity forcing of blocking flow fields. *Quart. J. Roy. Meteor. Soc.* **109**, 737–761.

Simmons, A. J., Wallace, J. M. and Branstator, G. W. 1983. Barotropic wave propagation and instability, and atmospheric teleconnection patterns. *J. Atmos. Sci.* **40**, 1363–1392.

Smith, T. M., Reynolds, R. W., Livezey, R. E. and Stokes, D. C. 1996. Reconstruction of historical sea surface temperature using empirical orthogonal functions. *J. Climate* **9**, 1403–1420.

Trenberth, K. E. 1985. Potential predictability of geopotential heights over the Southern Hemisphere. *Mon. Wea. Rev.* **55**, 54–64.

Trenberth, K. E. 1986. An assessment of the impact of transient eddies on the zonal flow during a blocking episode using localized Eliassen–Palm flux diagnostics. *J. Atmos. Sci.* **43**, 2070–2087.

Wallace, J. M. and Blackmon, M. L. 1983. Observation of low-frequency atmospheric variability. *Large-scale dynamical processes in the atmosphere* (eds. Hoskins, B. J. and Pearce, R. P.). Academic Press, pp. 55–94.

Zwiers, F. W. 1987. A potential predictability study conducted with an atmospheric general circulation model. *Mon. Wea. Rev.* **115**, 2957–2974.